Picosecond Laser-Induced Transient Grating Probe of the Mechanical Properties of High-Modulus Poly(*p*-phenylenebenzobisoxazole-2,6-diyl)

D. Narayana Rao, Yang Pang, Ryszard Burzynski, and Paras N. Prasad*

Department of Chemistry, State University of New York at Buffalo, Buffalo, New York 14214. *Received November 4, 1987; Revised Manuscript Received August 6, 1988*

ABSTRACT: The picosecond laser-induced transient grafting technique was used to determine the elastic constants of a predominantly uniaxial film of a rigid-rod polymer, poly(benzobisoxazole). By adjusting the grating angle, ultrasonic phonons in the frequency range 0.4–2 GHz were generated and their in-plane speed in various directions was measured. The speed was found to be independent of the phonon frequency in the range of frequency studied. The general Christoffel equation was used to fit the observed anisotropy of the acoustic velocity. This fit conveniently yielded various elastic moduli demonstrating the application of picosecond laser-induced transient grating methods for obtaining both longitudinal and shear components of elastic constants for an anisotropic medium.

Introduction

Laser-induced transient gratings have been observed in a wide variety of materials such as polymers, plasmas, dye solutions, and semiconductors, because of the ease with which the experiments can give diffusion constants, energy transport rates, and important mechanical properties.[1-8] These experiments are based on the spatial modulation of the optical properties of materials under study. Therefore, they are found to be very useful in the study of the anisotropy of the material as demonstrated in pioneer work by Fayer and co-workers.[1,2]

Organic polymeric systems containing π-electron conjugation show strong optical nonlinearities because of the π-electron contribution to the electrical susceptibility.[9,10] Particular interest has been shown in poly(*p*-phenylenebenzo[1,2-*d*:5,4-*d'*]bisthiazole-2,6-diyl) (PBT) and poly(*p*-phenylenebenzo[1,2-*d*:5,4-*d'*]bisoxazole-2,6-diyl (PBO) because of their rigid-rod-like molecular structure and high mechanical strength and stability.[11,12] They also possess high third-order optical nonlinearity.[13] The polymers can be formed as fibers or unoriented biaxial or uniaxial films. The rigid-rod polymers possess a very high modulus. Recently Smith et al.[14] used a novel arrangement, in which a pulse laser beam was focused into a very fine fiber of PBT to generate ultrasonic waves. From the speed of the ultrasonic wave, they obtained a very high value of 301 GPa for the Young's modulus of the PBT fiber.

We report the acoustic anisotropy of a PBO polymer film studied by the transient grating experiment which has been used to study the anisotropy of acoustic waves in crystals and thin films.[4-7,15] The anisotropy of the acoustic properties is studied by measuring the acoustic speed as a function of the orientation of the film. Fayer and coworkers[4,15] have investigated transient grating formation and acoustic wave propagation in an anisotropic medium. However, we apply the generalized Christoffel equation for a quantitative analysis of the anisotropy of observed acoustic speed. From the detailed theoretical analyses of the anisotropy of acoustic speed, we calculate various elastic constants of the polymer film. From our results we obtain both the longitudinal and shear components of the elastic constant tensor.

Experimental Section

The PBO polymer material, as-spun uniaxial fibrous film of thickness ~10 μm, was provided by Foster Miller, Inc. A good quality film was brown in color. This film was streched on a ring which in turn was mounted on an angular vernier scale to map out the orientational anisotropy of the acoustic velocity as the film is rotated.

The experimental set up is schematically illustrated in Figure 1. The laser system used for this investigation consists of a CW mode-locked and *Q*-switched Nd:YAG laser, with 150-ps pulse width in green, which pumps a synchronous cavity-dumped dye laser. The laser is operated at 500 Hz (*Q*-switching frequency of the YAG laser) over the wavelengths between 570 and 640 nm using R6G, DCM, and R640 dye solutions in ethanol. The pulses from the dye laser are 60–70 ps broad and 15 μJ in energy. However, a pulse energy of less than 4 μJ was used for the study by attenuating the beam with neutral density filters.

We have used a degenerate four-wave mixing (DFWM) configuration. The dye laser beam was split into two parts. One of the beams was sent through an optical delay line (with a maximum of 10-ns delay) and formed the backward beam I_3. The other portion was again split into two beams (I_1 and I_2) which were crossed at an angle θ in the film. A cross correlation was taken to set the arrival time of these beams to be the same. The forward (I_1) and backward (I_3) beams were aligned to be counterpropagating. A beam splitter was kept in the path of I_2 to collect the diffracted conjugate beam which was measured by means of a photodiode and a lock-in amplifier. The lock-in output was given to the Y arm of an *X*–*Y* recorder. To investigate the acoustic modulation of the diffracted signal, I_3 was delayed with respect to I_1 and I_2 by means of a retroreflector which was drawn along an optical bench. This provided a continuous scanning of the probe delay. A 10-turn potentiometer, driven by the moving retroreflector provided a voltage proportional to the probe delay. This voltage drove the *X* arm of the *X*–*Y* recorder. Thus when the delay line is run, a time-resolved plot of the diffracted signal is obtained. I_1, I_2, and I_3 are all kept vertically polarized and are in the horizontal plane. The details of the pump and probe beams configuration with respect to the film axes are shown in Figure 1b.

The speed of acoustic waves was measured every 10 deg in 19 different directions, covering exactly two quadrants, in order to check the sample symmetry. Each point was measured at least three times, and the final value used in our calculations was averaged over the number of measurements.

Results and Discussion

The theory of transient grating has been discussed in detail by Fayer.[1,2] Briefly reviewing it, the two time-coincident beams I_1 and I_2 crossing at an angle θ create a refractive index grating derived from various mechanisms. A third beam, I_3, is Bragg diffracted from this grating to generate the DFWM signal, I_4. The time decay of this grating can be monitored by measuring the DFWM signal I_4 as a function of time delay of beam I_3 with respect to beams I_1 and I_2.

The inset in Figure 2 shows the absorption spectrum of the polymer film in the visible range. Clearly, the wavelength of 578 nm is within the absorption profile. Under this resonance condition, the refractive index grating is

0024-9297/89/2222-0985$01.50/0

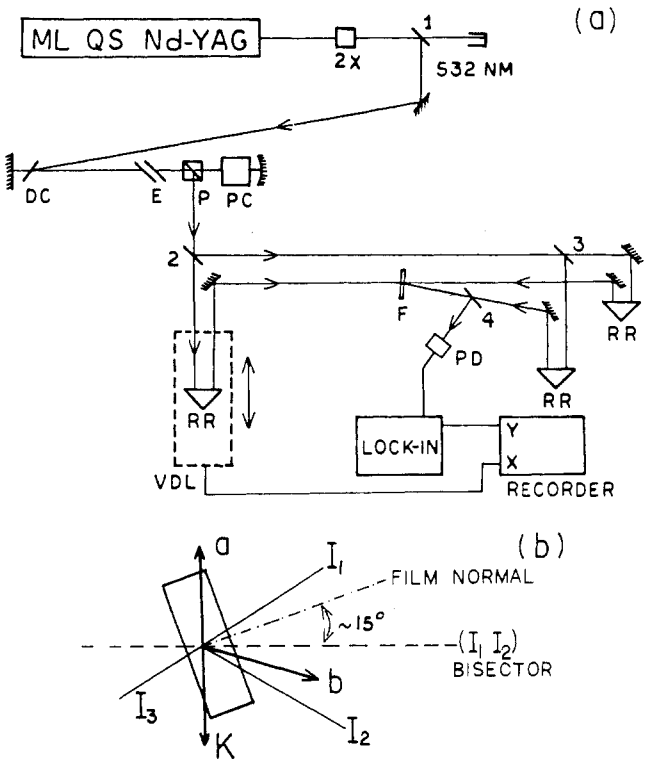

Figure 1. (a) Experimental setup for the transient grating measurement: PC = pockel cell, P = polarizer, E = etalon, DC = 1-mm flowing dye cell, 1, 2, 3, 4 = beam splitters, PD = photodiode, RR = retroreflector, F = sample, VDL = variable-delay line. (b) Configuration of the pump beams I_1 and I_2 and the probe beam I_3, with respect to the film axes. The crystallographic C axis is normal to the drawing plane. K is the grating wave vector.

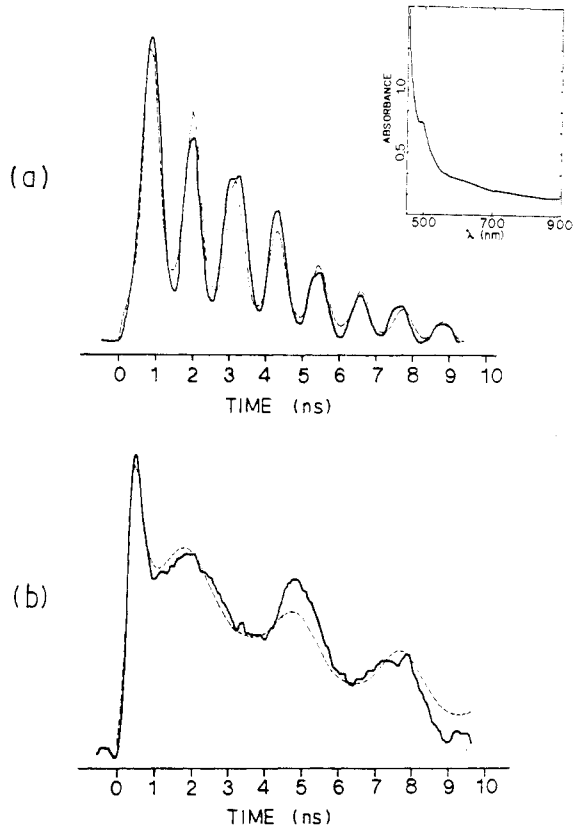

Figure 2. Acoustic modulation for $\theta = 11.9°$. (a) Sonic propagation along the fiber direction; (b) sonic propagation perpendicular to the fiber direction. Calculated curves are represented by dashed lines. Inset: Absorption profile of the PBO film.

mainly derived from material excitation. There are three important contributions. (i) Excited-state grating generated when the intensity modulation due to interference of the two crossing beams I_1 and I_2 leads to a corresponding modulation of the excitation number density. Since the refractive index of the material changes upon excitation, a refractive index grating is produced by the excited-state grating. This grating decays with a time constant twice that of excited-state decay constant, usually in nanoseconds. (ii) Thermal grating generated by local nonradiative relaxations causes temperature modulation and a corresponding refractive index modulation. The thermal grating decays in microseconds to multiseconds time range. (iii) Acoustic grating generated by density excursion causes a modulation of the refractive index. The wavelength of the acoustic wave is that of the grating spacing (discussed below). The DFWM signal diffracted from the acoustic grating undergoes a modulation with the acoustic period. This modulation is in the nanosecond range. Therefore, on the time scale of the decay of the excited state and the acoustic modulation, the thermal grating can be expected to provide a nearly constant background. The thermal grating can conveniently be probed in a separate experiment by using electronically synchronized nanosecond pulses from two separate laser sources.[16]

In addition to the resonant processes, a Kerr grating derived from nonlinear polarizations can also contribute. The electronic Kerr effect has a time response of subpicoseconds and does not pose any interference in the analysis of acoustic grating but the presence of orientational Kerr grating can interfere as discussed by Eyring and Fayer.[15]

Figure 2 shows the typical DFWM signal as a function of time delay of the backward beam I_3 when the grating (defined by the crossing beams I_1 and I_2) is created along two extremes of the film symmetry: (i) the grating is formed along the direction perpendicular to the draw direction (Figure 2a) and (ii) the grating is formed along the draw direction (Figure 2b). In each case the angle θ between I_1 and I_2 is 11.9°. In the latter case, the S/N observed is not as good because of large light scattering from the fibers. In each case we observe a modulated decay of the grating. Our result is similar to that reported by Nelson et al.,[17] where under a resonance condition, they observe a superposition of the excitation and acoustic gratings. The modulation of the DFWM signal is derived for the acoustic grating and is different for the two directions indicating anisotropy of the acoustic wave propagation. Although an acoustic grating can also be generated by a different mechanism, electrostriction,[1,2] under our experimental condition where the optical wavelength is within the absorption profile, the dominant mechanism is by local heating as discussed above. This assumption is also consistent with the observation that the acoustic amplitude follows a proportionality with the absorbance as the wavelength is changed from 578 to 640 nm.

To rule out the contribution due to orientational Kerr grating, DFWM experiments were carried out with different sets of relative polarizations of beams I_1, I_2, and I_3. Specially important is the case when the crossing beams I_1 and I_2 are orthogonally polarized. Under these conditions no acoustic grating is expected. We observed only a fast component (within the pulse autocorrelation width) due to the electronic Kerr effect; no orientational Kerr grating was observed. We conclude that the observed DFWM signal is derived from the excited state and acoustic gratings.

In the first step, we consider only the acoustic grating. In other words, we use the apparent modulation frequency to obtain the acoustic speed and analyze the anisotropy.

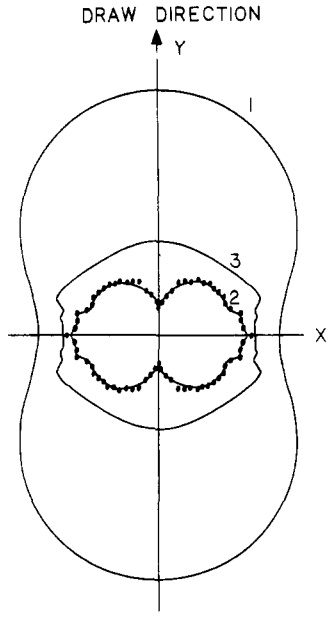

Figure 3. Polar plot of the acoustic velocity in the *ac* plane of the PBO film for the monoclinic symmetry. Theoretically calculated curves are represented by the solid lines: (1) quasi-longitudinal mode; (2 and 3) quasi-transverse modes. Triangles, experimental data points.

In the next step we use the calculated anisotropic speeds and theoretically simulate the DFWM signal diffracted from both the acoustic and excitation gratings. This theoretically simulated DFWM signal is compared with the experimentally observed behavior.

In the thermal mechanism of acoustic grating generation, the time delay between two successive diffraction peaks gives the acoustic period. The acoustic velocity can be derived as

$$v = \Lambda/d \tag{1}$$

where $\Lambda = \lambda/2 \sin \theta/2$ defines the acoustic wavelengths. Here, λ = the wavelength of the pump beams; θ = the angle between the pump beams I_1 and I_2; d = the acoustic period.

In an isotropic material the acoustic velocity is constant in all directions and varies as $(c/\rho)^{1/2}$, where c is the stiffness constant and ρ is the density of the material. In an anisotropic medium, on the other hand, the acoustic velocity varies in different directions.

It can be seen from Figure 3 that the measured acoustic velocity is smaller along the fiber and larger normal to it. According to the reported tensile moduli[18] (85 GPa along the fiber or draw direction and 6.5 GPa perpendicular to it), the velocities should be 7 km/s along the fiber and 2 km/s normal to it. We observed no such velocities.

The X-ray data[19] indicate that the film has a monoclinic symmetry with a = 5.64 Å, b = 3.58 Å, c = 12.07 Å, and γ = 100°. The b axis projects out of the film at an angle of 35° from the normal to the film plane. In our experimental set up (Figure 1b), the film is oriented at an angle of ~15° with respect to the bisector of I_1 and I_2. Such a tilt permits us to assume that the crystallographic axis b is oriented almost perpendicular to the grating wave vector k. This assumption reduces the three-dimensional problem to two-dimensional analysis in the *ac* crystallographic plane.

The general Christoffel equation is[20]

$$k^2(l_{iK}\mathbf{C}_{KL}l_{Lj})V_j = k^2\Gamma_{ij}V_j = \rho\omega^2 V_i \tag{2}$$

where $\Lambda_{ij} = l_{iK}\mathbf{C}_{KL}l_{Lj}$ is the Christoffel matrix, l_{iK} and l_{Lj} are the symmetry operators in the rectangular coordinates, and V_i and V_j represent the particle displacements along the directions i, j. $\mathbf{C}_{KL}$ is the stiffness matrix which has 21 components for a triclinic system.

We have attempted to solve the Christoffel equation in two steps because of the large number of unknown parameters ($\mathbf{C}_{KL}$). First, we used hexagonal symmetry, highest for the uniaxial system. Since the material is drawn along the c axis (chain direction), the fibers are oriented as fine rods along this axis. Such a configuration suggests use of the hexagonal symmetry. Next, we assumed the monoclinic symmetry as reported for this system and used the elastic constants obtained from the higher symmetry, as initial values, to solve exact Christoffel equations.

The general Christoffel equations can be written in the form

$$k^2\begin{pmatrix}\alpha & \delta & \epsilon\\ \delta & \beta & \xi\\ \epsilon & \xi & \gamma\end{pmatrix}\begin{pmatrix}V_x\\ V_y\\ V_z\end{pmatrix} = \rho\omega^2\begin{pmatrix}V_x\\ V_y\\ V_z\end{pmatrix} \tag{3}$$

where for monoclinic symmetry

$$\alpha = C_{11}lx^2 + C_{66}ly^2 + C_{55}lz^2 + 2C_{15}lzlx$$

$$\beta = C_{66}lx^2 + C_{22}ly^2 + C_{44}lz^2 + 2C_{46}lzlx$$

$$\gamma = C_{55}lx^2 + C_{44}ly^2 + C_{33}lz^2 + 2C_{35}lzlx$$

$$\delta = (C_{46} + C_{25})lylz + 2(C_{12} + C_{66})lxly$$

$$\epsilon = C_{15}lx^2 + C_{46}ly^2 + C_{35}lz^2 + (C_{13} + C_{55})lzlx$$

$$\xi = (C_{44} + C_{23})lylz + (C_{25} + C_{46})lxly$$

Here $lx = kx/k$, $ly = ky/k$, and $lz = kz/k$ are the direction cosines of the propagation direction. The crystallographic a axis coincides with x and the symmetry axis c coincides with y of the coordinate system. The particle velocity polarization,[16] given by

$$\frac{V_y}{V_x} = \frac{\xi(\alpha - \rho\omega^2/k^2) - \epsilon\delta}{\epsilon(\beta - \rho\omega^2/k^2) - \xi\delta} \tag{4}$$

defines the propagation mode as to be either a quasi-longitudinal or a quasi-transverse wave. Equation 4 can then be simplified to the following form:

$$V^3 - V^2\frac{1}{\rho}(\alpha + \beta + \gamma) + V\frac{1}{\rho^2}(\alpha\beta + \beta\gamma + 2\alpha - \delta^2 - \epsilon^2 - \xi^2) - \frac{1}{\rho^3}(\alpha\beta\gamma + 2\delta\epsilon\xi - \alpha\xi^2 - \beta\epsilon^2 - \gamma\delta^2) = 0 \tag{5}$$

where $V = \omega^2/k^2$ is the square of the phase velocity of the acoustic wave.

The above nonlinear equation is solved for the various constants by a nonlinear least-square fitting procedure in two steps: (1) We assume that acoustic waves propagate in the *ac* plane ($l_z = 0$). This gives us nine elastic moduli which are used as starting values in the final calculation. (2) We use correct angle between axis a and the I_1, I_2 bisector and solve eq 3 to produce all necessary elastic moduli for the monoclinic system. The values obtained are listed in the units of GPa: C_{11} = 16.33; C_{12} = 16.64; C_{13} = −0.49; C_{15} = −2.19; C_{22} = 84.0; C_{23} = 0.69; C_{25} = 2.01; C_{33} = 0.49; C_{35} = 19.11; C_{44} = 3.79; C_{46} = −4.18; C_{55} = 14.10; C_{66} = 10.34.

Figure 3 gives the theoretical fit for this model. It can be seen from the figure that the theoretical curve matches very well with the data points. Our calculated value of C_{22} (84.0 GPa) is in excellent agreement with the reported value[18] for the tensile modulus along the fiber direction (symmetry axis).

The solution to eq 5 gives three phase velocities, V_1, V_2, and V_3. The experimental data are in good agreement with the V_2 values. The calculation of particle velocity polarizations by eq 4 shows that V_2 and V_3 are quasi-transverse and that V_1 is quasi-longitudinal. Figure 3 also shows the polar plots for all three calculated phase velocities.

We tried to observe the high-velocity quasi-longitudinal component along the fiber direction, which should be equal to $(C_{22}/\rho)^{1/2}$, i.e., around 7.5 km/s. We were unsuccessful in this effort. This could be because of the following: (i) Our laser pulses are around 70 ps, and the ratio between the expected acoustic period to pulse width is around 5. This would reduce the difference between the acoustic minima and maxima.[21] However, even with such long pulses, the acoustic period can be observed if θ is small enough, about 2°. Although experimentally this does not create any problem, difficulties arose from the radiative background due to the light scattering from polymer fibers which made the conjugate signal detection impossible. (ii) The nonradiative relaxation could be slower. We plan to resolve this, by working at a much shorter pulse width or alternatively by using two-color transient grating experiments.

Now we attempt to make a more quantitative analysis of the observed DFWM signal by taking into consideration that acoustic modulation is superimposed on a slowly decaying excited-state grating. As has been discussed by Nelson et al.,[3] the grating can be of two types: a phase grating (change in the real part of the refractive index) and an amplitude grating (change in the imaginary part of the refractive index). For the case of a thermal acoustic grating superimposed on the excited state grating, one can describe the grating efficiency as[2]

$$\eta \propto E_A^2 + (E_p + A_p)^2 \tag{6}$$

Here E_A and E_p are the excited-state amplitude and phase grating contributions; A_p is the acoustic phase grating contribution. E_p vanishes at the absorption maximum.

Now we make the assumption that only the excited-state amplitude grating and the acoustic phase grating contribute. The validity of this assumption will be tested by the fit of the theoretically simulated DFWM signal with that experimentally observed. Under this approximation

$$\eta \propto (E_A^2 + A_p^2) \tag{7}$$

we can write the decay of the DFWM signal as

$$I_4 \propto [1 - \exp(-t/\tau_p)]^2\{A[\exp(-t/\tau)]^2 + B[\exp(-\Gamma t) \times (1 - \cos(\Omega(t - t_0)) + \delta)]^2\} \tag{8}$$

In the above expression τ_p is the pump pulse duration to include the pump pulse convolution which overlaps the first acoustic peak. Γ is the damping factor for the acoustic oscillation. The terms t_0 and δ are the phase and background offsets, respectively. If the acoustic speed (the corresponding frequency Ω) for the transverse mode V_2 is used and the damping constant $\Omega = 2.3 \times 10^8$ s^{-1} is adjusted, eq 8 describes the observed DFWM signal time behavior quite well. This theoretical curve is also shown in Figure 2 (top). Since the focus of the present work is only on acoustic speed and elastic constants, we do not discuss the excited-state grating parameters and the acoustic damping behavior.

The DFWM time behavior along the fiber direction (Figure 2 (bottom)) is much more complicated. First, the data along this direction are not as good due to the problem with background light scattering. Second, the curve appears to have more than one Fourier component. The spacing between the first and second peaks is not the same as those between the following peaks. A better fit was obtained when we assumed that the two quasi-transverse acoustic modes V_2 and V_3 (whose frequency and speeds have been discussed above, curves 2 and 3 in Figure 3) contribute together with the excited-state grating. In such a case the acoustic contribution in eq 8 consists of two terms with two different sets of B_i, Γ_i, Ω_i, t_{0i}, and δ_i. The best theoretical fit we could obtain is shown in Figure 2 (bottom). Although the theoretically simulated curve does not correlate with the experimental data as well as it does for the transverse direction (Figure 2, top), in view of the poor S/N ratio for this direction, we consider the fit adequate. This fit yields a more rapid attenuation ($\Gamma = 5.5 \times 10^9$ s^{-1}) of the transverse component V_3 compared to that for V_2 such that the V_3 component essentially contributes only the first peak. From our theoretical analysis, it appears that our observed time behavior of the DFWM signal is consistent with the assumption of superposition of the excited-state amplitude grating and the acoustic phase grating. It also is consistent with the elastic constant analysis discussed above.

The polymer fibers are not oriented exactly along the draw direction. The X-ray analysis shows that fibers are rather distributed around the symmetry axis c within the angle of ±5°.[19] Our light-scattering analysis, however, showed that this angle is ±15°. For the particular case of propagation along the x and y axes, the quasi-transverse mode becomes the pure transverse one. As indicated in ref 5, in a thermal mechanism, there should not be a pure transverse mode. We feel that since the fibers are distributed around the c axis, there is not clear-cut c axis but only a distribution and hence we still see a quasi-transverse mode along the x and y axes.

The large value for C_{22} indicates that the film is predominantly oriented along the molecular chain axis (c) and thus supports the assumption of a monoclinic symmetry used in the derivatization of the elastic constants. The large value of C_{22} also supports the fiberlike structure and strong intramolecular interactions along the molecular axis (draw direction). The lower value for C_{11} indicates weaker intermolecular interactions perpendicular to the draw direction (fiber axis) compared to the intramolecular interaction indicated by C_{22}.

To look at the effect of acoustic frequency on the velocity, we have varied the angle between the pump beams from 5° to 26°. This leads to an acoustic frequency range 0.4–2 GHz. A plot of $\lambda/2 \sin \theta/2$ versus the observed modulation, d, yields a straight line (Figure 4) with a slope equal to the velocity of sound. This indicates that the acoustic speed is independent of the acoustic frequency for this range. For various orientations of the film, the velocity follows the same profile as that of Figure 3. We see no high-velocity component even after changing the pump wavelength from 575 to 640 nm.

In conclusion the study of orientational anisotropy of the acoustic velocity in the film leads us to the precise measurement of the elastic constants which are very difficult to obtain by the standard techniques. The results demonstrate the ease with which the technique can be applied to the study of the mechanical properties of thin polymeric films. By measuring of quasi-mode velocity in different directions of the film, we obtained both the longitudinal and *shear* components of the elastic constants of the polymer film. By simply changing the angle between the two pump beams, the acoustic frequency has been varied between 2 and 0.4 GHz. The transient grating technique should prove to be very useful for the study of

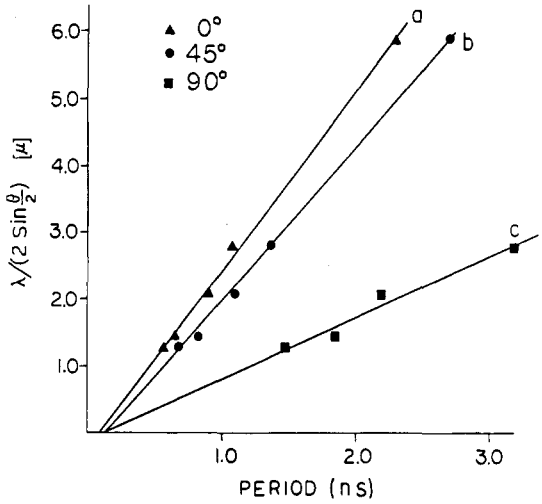

Figure 4. Plot of ($\lambda/2 \sin \theta/2$) in units of micrometers versus the observed acoustic modulation period for various angles.

the mechanical properties of oriented polymer films.

Acknowledgment. We thank R. Lusignea of Foster Miller, Inc., for providing us with the PBO samples and the X-ray and tensile modulus data as well as for helpful discussions. We also thank Dr. W. W. Adams and Dr. I. Goldfarb of Polymer Branch, Air Force Wright-Aeronautical Laboratories; Dr. D. R. Ulrich of Air Force Office of Scientific Research; Professor M. D. Fayer of Stanford University; and Professor K. A. Nelson of M.I.T. for helpful discussions. This work was supported by the Air Force Office of Scientific Research Contract F4962087C0042.

Registry No. PBO, 60871-72-9.

References and Notes

(1) Fayer, M. D. *Annu. Rev. Phys. Chem.* **1982**, *33*, 63.
(2) Fayer, M. D. *IEEE J. Quantum Electron.* **1986**, *QE-22*, 1437.
(3) Nelson, K. A.; Miller, R. J. D.; Lutz, D. R.; Fayer, M. D. *J. Appl. Phys.* **1982**, *53*, 1144.
(4) Eyring, G.; Fayer, M. D. *Biophys. J.* **1985**, *47*, 37.
(5) Nelson, K. A.; Fayer, M. D. *J. Chem. Phys.* **1980**, *72*, 5202.
(6) Nelson, K. A.; Casalegno, R.; Miller, R. J. D.; Fayer, M. D. *J. Chem. Phys.* **1982**, *77*, 1144.
(7) Eyring, G.; Fayer, M. D. *J. Chem. Phys.* **1984**, *81*, 4314.
(8) Rao, D. N.; Burzynski, R.; Mi, X.; Prasad, P. N. *Appl. Phys. Lett.* **1986**, *48*, 387.
(9) *Nonlinear Optical Properties of Organic and Polymeric Materials*; Williams, D. J., Ed.; ACS Symposium Series 233; American Chemical Society: Washington, DC, 1983; and references therein.
(10) *Nonlinear Optical and Electroactive Polymers*; Prasad, P. N., Ulrich, D. R., Eds.; Plenum: New York, 1988.
(11) Wolfe, J. F.; Loo, B. H.; Arnold, F. E. *Macromolecules* **1981**, *14*, 915.
(12) Adams, W. W.; Helminiak, T. E. In *Science of Ceramic Chemical Processing*; Hench, L. L., Ulrich, D. R., Eds.; Wiley: New Yokr, 1986; p 444.
(13) Rao, D. N.; Swiatkiewicz, J.; Chopra, P.; Ghoshal, S. K.; Prasad, P. N. *Appl. Phys. Lett.* **1986**, *48*, 1187.
(14) Smith, J. J.; Jiang, H.; Eby, R. K.; Adams, W. W. *Polym. Commun.* **1987**, *28*, 14, and references therein.
(15) Eyring, G.; Fayer, M. D. *J. Chem. Phys.* **1984**, *81*, 4314.
(16) Cong, P.; Pang, Y.; Prasad, P. N. *J. Chem. Phys.* **1986**, *85*, 1077.
(17) Nelson, K. A.; Lutz, D. R.; Fayer, M. D. *Phys. Rev. B: Condens. Matter* **1981**, *24B*, 3261.
(18) Lusignea, R., Foster Miller Data on Tensile Modulus, private communication.
(19) Thomas, E. L.; Saruyama, Y. X-ray Diffraction Characterization of PBO Films, communicated to Foster Miller.
(20) Auld, B. A. *Acoustic Fields and Waves in Solids*; Wiley-Interscience: New York, 1973; Vol. 1.
(21) Miller, R. J. D., private communication.

Notes

Copolyimidines. 2. Copoly(imidine-imides) from 3,5-Dibenzylidenepyromellitide, 4,4'-Diaminodiphenyl Ether, and Various Dianhydrides

MITSURU ARAI, PATRICK E. CASSIDY,* and JAMES M. FARLEY

Department of Chemistry, Southwest Texas State University, San Marcos, Texas 78666.
Received May 10, 1988

Introduction

Processable, high-termperature polymers are still very desirable materials, especially in the aerospace and electronic industries. Applications of these polymers both as neat resins and as matrix resins for composite materials are numerous. A review of properties and syntheses of high-temperature polymers has been reported.[1]

Polyimides are a well-known class of thermally stable polymers which show excellent mechanical and electrical properties over a wide temperature range, as well as good chemical resistance.[2] However, applications of polyimides are occasionally limited due to their poor solubility and molding properties.

Polyimidines constitute a relatively new class of polymers which were designed to have improved processability while retaining desirable physical and chemical properties.[3-16] These polymers are structurally similar to polyimides but possess bulky, pendant groups on the backbone which greatly enhance solubility. One inherent drawback to polyimidines has been low molecular weight and therefore an inability to form good films or fibers. In a previous paper,[17] we reported a new class of thermally stable polymers, namely copoly(imidine-imides), which was designed to have superior properties over either homopolymer. These copolymers were prepared by the sequential condensation of 3,5-dibenzylidenepyromellitide, *m*-xylylene-diamine, and various dianhydrides. The resulting copolymers were soluble in polar aprotic solvents and possessed sufficient molecular weight which allowed solution casting of tough films with moderate mechanical properties. Their thermal stabilities ranged from 410 to 475 °C by TGA.

This paper reports the synthesis and properties of copoly(imidine-imides) which do not contain any aliphatic linkages in the polymer backbone. In contrast to polymers with benzylene groups in the backbone, a wholly aromatic system affords a more rigid structure and should show improved thermal stability and mechanical properties.

Results and Discussion

Synthesis of Copoly(imidine-imides). A series of three copoly(imidine-imides) was prepared from the co-

0024-9297/89/2222-0989$01.50/0